1 Host CD59 Potentiates the Type III Secretion System in *Yersinia pseudotuberculosis*

2

3 Kristen J. Davis[1,2,#], Kerri-Lynn Sheahan[1,3,*], Connor S. Murphy[1,3,*] and Ralph R. Isberg[1,3]

4

5 [1]Department of Molecular Biology and Microbiology

6 [2]Graduate Program in Molecular Microbiology, Tufts University Graduate School of Biomedical

7 Sciences

8 [3]Tufts University School of Medicine, Boston, MA, USA

9

10 Running title: CD59 contributes to T3SS Function in *Y. pseudotuberculosis*

11

12 [#]Address correspondence to Ralph.Isberg@tufts.edu

13 [*]Present addresses: Kerri Sheahan, Obsidian Therapeutics;

14 Connor Murphy, Graduate School of Biomedical Sciences and Engineering, University of Maine

15

Abstract

Type III secretion systems (T3SS) play critical roles in disease for many Gram-negative pathogens. For *Yersinia pseudotuberculosis* (*Yptb*), the machinery delivers the Yop bacterial effectors into host cells, misregulating cytoskeletal components and sabotaging immune defenses. Although the structural details of T3SS assembly have been studied extensively, intimate interactions between the T3SS components and the surface of the target host plasma membrane are poorly characterized. A previous RNA interference (RNAi) identified the GPI-linked surface protein CD59 as a critical host component that supports T3SS translocation pore formation and effector movement into the host cytosol. We show here that depletion and increased levels of CD59 reduced *Yptb* T3SS pore formation and Yop translocation into host target cells. In contrast, enzymatic removal of all GPI-linked surface proteins from wild type cells prior to *Yptb* infection had no effect on T3SS function, indicating that neither CD59 nor other GPI-linked proteins were receptors for the T3SS machinery. Consistent with its importance in supporting the T3SS function, efficient bacterial effector-mediated focal adhesion disassembly was dependent on CD59. Depletion of CD59 interfered with the rearrangement of the lipid raft marker GM1 that occurs after *Yptb* adhesion to host cells, indicating that CD59 supports lipid microdomain dynamics. Consistent with a role in modulating lipid composition, the loss of CD59 resulted in the accumulation of phosphatidylcholine lipids, alteration in fatty acid chain lengths and fatty acid saturation levels. This work points to a role for CD59 in maintaining plasma membrane dynamics necessary to support efficient T3SS function.

39 **Introduction**

40 Pathogenesis of *Yersinia pseudotuberculosis* (*Yptb*) requires the Type III Secretion
41 System (T3SS), which is used to deliver bacterial effectors into host cells that misregulate host
42 signaling pathways and are required to evade innate immune responses (1-3). The T3SS is
43 encoded on a ~70kb virulence plasmid present in the three species of *Yersinia* that infect humans:
44 the enteropathogenic *Y. enterocolitica* and *Y. pseudotuberculosis*, and the causative agent of
45 bubonic plague, *Y. pestis* (4-6). The structure and function of the secretion apparatus is well-
46 conserved among many Gram-negative pathogens, with the *Yersinia* syringe-like nanomachine
47 delivering bacterial effector proteins, called Yops (*Yersinia* outer proteins), into the host cell
48 cytosol (2, 7). There is a core effector set of six Yops, with YopT specifically absent in most *Yptb*
49 strains (including YPIII, the strain used in this study) (8, 9). Although much work has been done
50 to describe the structure and function of the T3SS, how the host cell supports the function of the
51 apparatus is largely unknown.

52 Yops act to prevent engulfment by professional phagocytes and interfere with reactive
53 oxygen killing, allowing successful extracellular bacterial replication and survival in host tissues,
54 even with neutrophil-adherent bacteria (3, 10). YopE, for example, is a GTPase activating protein
55 (GAP) that inactivates Rho-family GTPases such as RhoA, Cdc42, and Rac that regulate actin
56 cytoskeletal function required for phagocytosis and production of reactive oxygen species via
57 assembly of the NADPH oxidase complex (11, 12). Interestingly, it has been shown that host cell
58 Rho GTPase activity is initially required for efficient translocation of Yops (13) emphasizing that
59 modulation of the actin cytoskeleton plays multiple roles in establishing disease. Several other
60 host factors have been identified that are important for T3SS function, including host cell

61 sulfation and fucosylation in *Vibrio parahaemolyticus*, and DNAJC5 in *Pseudomonas*
62 *aeruginosa*, which acts as a chaperone for effector translocation (14-16).
63 We previously identified mammalian proteins important for the function of YopE using a
64 mammalian siRNA knockdown library and a FRET-based Rho GTPase biosensor (17). The
65 identified host proteins in the screen included the chemokine receptor CCR5, shown to affect
66 T3SS function, but also identified a number of other proteins involved in cell adhesion,
67 signaling, and membrane trafficking (17). These included CD59, a glycosyl-phosphatidylinositol
68 (GPI)-anchored protein found on the surface of most mammalian cell types that functions as a
69 self-recognition marker to protect against complement attack (18). The presence of CD59 on
70 mammalian cells prevents the oligomerization of complement proteins into membrane attack
71 complexes (MACs) in response to activation, whereas microorganisms with no such defense are
72 targeted for destruction (19-21). CD59 is also a direct receptor for some bacterial cholesterol-
73 dependent pore-forming cytolysins, making it of interest for the analysis of a role in forming the
74 T3SS translocation channel (22, 23). In addition, CD59 is an important component of
75 microdomains in the plasma membrane, known as lipid rafts, that are important for critical cell
76 functions such as membrane trafficking, chemokine signaling, and immune cell activation (24).
77 Studies in several similar pathogens including *Shigella*, EPEC, and *Salmonella* have revealed
78 that functional lipid rafts on the host cell surface play an important role in supporting microbial
79 adhesion, T3SS translocon pore insertion, and delivery of translocated effector substrates (25-
80 27).
81 In this study, we show that cells lacking CD59 are associated with aberrant mobilization
82 of host cell plasma membrane components in response to *Yptb*-target cell contact resulting in

83 defective effector translocation and translocon pore formation. These results also argue that
84 CD59 is unlikely to act as a direct receptor that engages the T3SS.
85
86 **Results**
87 **Knockout and increased surface expression of host cell CD59 result in inefficient pore**
88 **formation by *Yptb***
89 A pooled shRNA knockdown approach, used to detect mammalian proteins important for
90 *Yptb* YopE function, identified the plasma membrane protein CD59 as a candidate for playing a
91 role in Yop translocation (17). Verification of the hit revealed that when host cell CD59 was
92 knocked down by shRNA, significant T3SS defects were evident, based on a defect in YopB/D-
93 dependent pore formation and translocation assays performed on a second translocated effector,
94 YopH (17). These data were consistent with a general defect in T3SS translocator function rather
95 than direct modulation of YopE activity. To pursue these results further, a cloned CD59 knockout
96 line (CD59 KO) was constructed in HEK 293T cells using the LentiCRISPRv2 vector (28). Cell
97 surface labeling of the CD59 KO cell line with anti-CD59-FITC followed by analysis with flow
98 cytometry resulted in fluorescence that was indistinguishable from an isotype control (Figure
99 1A). In contrast, WT HEK 293T cells, showed robust labeling with the anti-CD59-FITC
100 conjugate (Figure 1A).
101 To determine if *Yptb* challenge of the CD59 KO cell line exhibited translocation defects
102 similar to the shRNA knockdown, a T3SS pore formation assay was performed. Once injected
103 into a target cell, the Yop effectors downmodulate pore formation to prevent immediate
104 cytotoxicity of the host (29). Therefore, a Δ*yopHMOJE* (YPIIIΔ5) strain that lacks all regulatory
105 Yops and exhibits hyper pore-forming activity was used to measure pore formation. This assay

106 utilizes uptake of a fluorescent amine-reactive membrane-impermeant probe, measuring FITC
107 incorporation as a proxy for pore formation (17).
108 The *Yersinia* translocon pore complex comprises the two hydrophobic pore proteins
109 YopB and YopD, as well as the hydrophilic scaffolding protein LcrV, which localizes to the
110 needle tip (7). A *yopB* mutant strain (YPIIIΔB) lacking the major translocon pore protein YopB
111 is unable to form pores in the host cell plasma membrane and serves as a negative control for
112 pore formation and translocation (10). WT and CD59 KO cells were challenged with YPIIIΔ5 or
113 YPIIIΔB at MOI = 25 for 2 hours and analyzed for FITC incorporation by flow cytometry. WT
114 and CD59 KO cells infected with the YPIIIΔB mutant were intact and unperturbed as shown by
115 their similarly low background level of fluorescent labeling (Figure 1B). In the WT cells infected
116 with YPIIIΔ5, two distinct right-shifted populations were observed that were labeled by the
117 probe. The peak furthest to the right shows maximum cytotoxicity while the wider shouldered
118 peak represents varying degrees of pore formation. The CD59 KO cells also showed these two
119 populations, but there was a distinct shift toward lower probe incorporation on these peaks,
120 indicating that cells lacking CD59 were less susceptible to pore formation by YPIIIΔ5 compared
121 to WT cells (Figure 1B).
122 To further interrogate the effect of CD59 expression levels on the host plasma membrane
123 on *Yptb* T3SS function, WT CD59 was introduced into the CD59 KO cell line to evaluate if pore
124 forming activity could be restored. Human CD59 expressed from the mammalian expression
125 vector pcDNA3.1+ was transfected into CD59 KO 293T cells, and monoclonal populations were
126 isolated after antibiotic selection. Two clones exhibiting CD59 levels similar to WT (KOpCD59-
127 WT1 and KOpCD59-WT2) as well as two clones with increased surface levels of CD59
128 (KOpCD59-OE1 and KOpCD59-OE2) were identified (Figure 1C). Each of these clones, along

129 with the WT and KO cell lines, were assayed for pore formation after infection by YPIIIΔ5.
130 Interestingly, both CD59 clones with increased surface levels of CD59 showed similar resistance
131 to pore formation by YPIIIΔ5 compared to what was observed with the KO cells. The only clone
132 that restored the degree of pore formation seen in WT cells was one of the clones that exhibited
133 WT levels of surface CD59 (Figure 1D). Although clones could be isolated in which pore
134 formation by YPIIIΔ5 could be restored, there appeared to be confounding effects that prevented
135 effective complementation. In addition to the clones shown here, random screening of several
136 overproducing clones failed to show the same level of pore formation as was exhibited with the
137 WT1 clone (Figure 1D).

138 Phenotypic variation was observed among the CD59 KO and KOpCD59 clones upon
139 prolonged passaging as another confounding problem, so strategies were sought to overcome this
140 issue. CD59 is one of the most abundant GPI-linked proteins, so knocking it out may select for
141 suppressor mutations or unpredictable changes in regulatory patterns that could be propagated
142 over many passages. For this reason, we chose to continue investigating the role of CD59 in *Yptb*
143 T3SS function using transient siRNA knockdown. Efficient CD59 knockdown was achieved 72
144 hours post-transfection using mixed pools of siRNAs directed against CD59 (Materials and
145 Methods; Figure 2A).

146 The pore forming assay measures loss of cellular viability, which may have further
147 complicated the analysis. To evaluate siCD59 knockdown populations using a strategy that does
148 not require loss of membrane integrity, T3SS function was assessed by measuring Yop
149 translocation into host cells, detected by assaying for YopE-TEM (or YPIIIΔB YopE-TEM)
150 translocation using a β-lactamase reporter strain followed by FACS analysis (30). After a 1hr
151 infection at MOI = 1, HEK 293T cells were loaded with CCF4-AM, a FRET-based β-lactamase

152 substrate that readily enters the host cells as detected by a green fluorescence signal at 515nm
153 after 409nm excitation. Translocation of YopE-TEM was detected by cleavage of the TEM
154 substrate which results in a blue fluorescence signal at 450nm using the same excitation
155 wavelength. Translocation, therefore, was visualized by a green-to-blue shift and calculated as
156 the ratio of the fluorescence intensity of 450nm emission relative to 515nm emission after
157 excitation with the 409nm laser line. This was displayed with contour plots of the blue vs. green
158 channels (Figure 2B). Green cells were gated with the YPIIIΔB YopE-TEM negative control
159 (Figure 2B, left panel). After a 1hr infection of siNT cells with YopE-TEM, approximately 65%
160 of the gated blue vs. green cells shifted to the blue gate, indicating robust translocation (Figure
161 2B, middle panel). In the siCD59 infection (Figure 2B, right panel) this was reduced to 45% of
162 the gated cells, indicating no detectable translocation in a large fraction of the cells. The total
163 translocation in the population was reduced by about 50% as well, based on the ratio of the total
164 fluorescence intensity at 450nm to 515nm in siCD59 knockdown cells from triplicate samples
165 (Figure 2C).
166
167 **Host cell CD59 indirectly supports *Yptb* T3SS-dependent pore formation**
168 Intermedilysin (ILY) is a bacterial-encoded cholesterol-dependent pore-forming toxin
169 (PFT) from *Streptococcus intermedius* that requires CD59 as a receptor (22). The wild-type form
170 of this protein (ILY^{WT}) forms pores in the host cell membrane, whereas a mutant version that is
171 fixed in a prepore conformation (ILY^{PP}) binds CD59 without forming an active pore, leaving the
172 host cell membrane intact (31). The *Yptb* translocon pore proteins YopB and YopD share
173 physiological properties with PFTs (32) and we hypothesized that if the *Yptb* translocon pore

174 interacts with CD59 in a similar manner to ILY, then ILY^{PP} binding to CD59 will block T3SS-
175 dependent pore formation.

176 His-ILY^{WT} and His-ILY^{PP} were expressed in *E. coli* BL21 (DE3) and purified (Materials
177 and Methods). HEK 293T cells were then pretreated with ILY^{PP} or mock buffer control,
178 challenged with ILY^{WT}, and assayed for pore formation. Cells that were mock-treated and
179 challenged with ILY^{WT} exhibited high levels of pore formation, confirming that the ILY^{WT} was
180 functioning properly (Figure 3A). Cells pretreated with ILY^{PP} were protected from pore
181 formation, indicating that the mutant protein successfully bound the CD59 receptor and blocked
182 ILY^{WT} (Figure 3A). To determine if ILY^{PP} could block *Yptb* T3SS-dependent pore formation,
183 293T cells were pretreated with ILY^{PP} for 1 hour and then challenged with YPIIIΔ5 or YPIIIΔB
184 at MOI = 25 for 2 hours (Figure 3B). There was no difference in pore formation among the ILY^{PP}
185 pretreated and mock-treated cells, indicating that if there was a direct interaction between CD59
186 and the T3SS machinery, it did not occur at the ILY binding site.

187 To eliminate the possibility that an insufficient quantity of ILY^{PP} was added to the cells to
188 block all binding sites, cells were treated with phospholipase C (PLC), an enzyme that cleaves
189 above the phosphoinositol group of the GPI-anchor, releasing CD59 and other GPI-linked
190 proteins. WT 293T cells were pretreated with PLC, challenged with YPIIIΔ5, then assayed for
191 pore formation. This strategy depleted GPI-linked proteins based on detection of these linkages
192 with Alexa488-conjugated proaerolysin, as PLC treatment resulted in a distinct decrease in
193 fluorescence compared to the mock-treated cell population. After the 2 hr infection with
194 YPIIIΔ5, there was no significant difference in pore formation between the PLC-treated and
195 mock-treated cells (Figure 3D). This provides clear evidence that CD59 is not a receptor for

196 T3SS translocation, and additionally rules out any other GPI-linked protein for this potential
197 receptor role.
198
199 **CD59 is required for efficient focal adhesion disruption by *Yersinia***
200 Upon contact with host cells, the bacterial invasin and YadA proteins engage and activate
201 host β1-integrin receptors, leading to recruitment of signaling and cytoskeleton-binding proteins
202 such as paxillin, focal adhesion kinase (FAK), Src-family kinases, and p130Cas. These protein
203 complexes at the integrin cluster sites are called focal adhesions (33). Lipid raft domains are also
204 recruited and involved in integrin clustering and likely promote the assembly and reinforcement
205 of FAs (34). *Yersinia* can disrupt these focal adhesions by translocating the YopH protein tyrosine
206 phosphatase, blocking phosphotyrosine signaling and the actin rearrangements that drive
207 phagocytosis (35-37). YopH has many host targets, including FAK, p130Cas, and Src-family
208 kinases at focal adhesion sites (33, 38, 39), as well as the tyrosine kinase Lck and the LAT
209 adapter in T cells (36, 40).
210 To determine whether CD59 activates focal adhesion formation, similar to its activation
211 of cytoskeletal regulators in T cells (40), an anti-phosphotyrosine (pTyr) antibody was used to
212 assess whether reduced CD59 levels interfere with YopH tyrosine phosphatase activity during
213 *Yptb* infection. HeLa cells were knocked down with either siCD59 or the siNT control for 72
214 hours, challenged with *Yptb gfp*$^{+}$ bacteria, fixed, and immunostained with anti-pTyr. Focal
215 adhesions appear as brightly stained fiber-like bundles, numerous in both siCD59 knockdown
216 and siNT control cells in the absence of infection (Figure 4A). Upon challenge with WT
217 *Yersinia*, focal adhesions were readily disassembled in the CD59-positive siNT control cells, as
218 evidenced by the absence of large bundles and increased puncta (Figure 4B, left panel). This

219 process was inefficient in the siCD59 knockdown cells, as larger focal adhesions were still
220 visible (Figure 4B, right panel) compared to the siNT control cells.
221 Focal adhesions were identified and measured by an image analysis routine that
222 distinguishes edges to identify focal adhesion particles, based on a previously published
223 workflow (41). The average size of each focal adhesion and the total sum of pixels identified per
224 cell were significantly lower in CD59 positive control cells compared to the CD59 knockdown
225 (Figure 4C and D, respectively) indicating that CD59 is required for efficient disruption of these
226 host cell signaling assemblies. This is consistent with a defect in YopH accumulation and/or
227 targeting of focal adhesions after bacterial contact with host cells deficient for CD59.
228
229 **Depletion of CD59 alters GM1 trafficking after *Yptb* challenge**
230 Our results indicate that the *Yptb* T3SS is highly sensitive to alterations in CD59 plasma
231 membrane content. CD59 is enriched in microdomains in the cell membrane where cholesterol,
232 glycosphingolipids, GPI-linked proteins, and signaling proteins are densely associated (24).
233 These receptor-rich microdomains are thought to be highly dynamic and may transiently
234 rearrange in response to activating signals, such as the adhesion of a pathogen (42). As CD59
235 plays an indirect role in supporting *Yptb*-dependent T3SS function (Figure 3), the dynamics of
236 host cell membrane organization were investigated as a function of CD59 expression, probing for
237 microdomains. Cholera toxin B subunit (CtxB) binds to the glycosphingolipid GM1 in lipid
238 microdomains and can be used to detect altered microdomain distribution in response to bacterial
239 binding (43). Therefore, the GM1 probe AlexaFluor594-CtxB was added to the cell culture
240 medium immediately before *Yptb* challenge of cells that had been siRNA-depleted of CD59 for

241 72 hr prior to infection, using nontargeting siRNA as the control (siCD59 and siNT respectively;
242 SmartPools™, Dharmacon).
243 In the absence of *Yptb* infection, GM1 was notably localized to the perinuclear region in
244 control CD59-positive cells (Figure 5A). After CD59 depletion, however, GM1 puncta began to
245 accumulate at the cell periphery when compared to the siNT control cells (compare Fig. 5A to
246 5B, two examples). When challenged with the T3SS-deficient *Yptb* ΔB mutant, there was largely
247 no change compared to the uninfected controls (Figures 5D and C, respectively). Strikingly,
248 when siNT cells were challenged with WT *Yptb*, any residual peripheral localization was largely
249 lost and GM1 was exclusively perinuclear (Figure 5E, two examples of tight perinuclear
250 staining). This is in stark contrast to the CD59 knockdown cells, in which perinuclear
251 localization disappeared and GM1 puncta were dispersed across the whole cell surface (Figure
252 5F), consistent with a defect in GM1 trafficking. Therefore, the absence of CD59 causes
253 dispersion of GM1 gangliosides in response to an intact T3SS. This phenotype was not due to
254 alterations in surface localization of GM1 gangliosides, as flow cytometry of cells probed for
255 GM1 indicted that CD59 knockdown had no effect on surface levels of GM1 compared to siNT
256 control cells (Figure S2). Diffuse punctate localization of GM1, therefore, is correlated with
257 defects in supporting T3SS function.
258
259 **Loss of CD59 perturbs lipid composition of plasma membrane**
260 To investigate if the loss of CD59 results in changes of lipid composition, cells were
261 extracted in 2:1 chloroform:methanol and samples were analyzed by mass spectrometry to
262 identify lipid components using LC-MS/MS (44). Principal component analysis (PCA) of mass
263 spectrometry peak data normalized by percent abundance within each sample shows suitable

264 separation of samples by cell type (Figure 6A). The two most abundant lipid classes in both lines
265 were phosphatidylcholine (PC) and phosphatidylethanolamine (PE). The bulk sum carbon (C)
266 composition of the acyl chains for PC species detected by mass spec is shown in Figure 6B,
267 indicated by total number of carbons as a percentage sum of all PC lipids for each sample. Acyl
268 chains totaling 34 bulk sum carbons were by far the most abundant PCs, and the WT had
269 significantly more of these species as compared to CD59 KO cells ($P<0.05$). Interestingly, the
270 KO cells exhibited a greater number of very short (<30 bulk sum carbons) and very long acyl
271 chains (>42 bulk sum carbons) (Figure 6B). A similar trend was found in PE species (Figure 6C).
272 WT cells had more of the most abundant 34C species among PE, while greater numbers of
273 longer (>35C) and shorter (<35C) acyl chains were detected in CD59KO cells compared to WT
274 cells (Figure 6C).
275 Sphingomyelin (SM) is enriched in ordered lipid raft domains and has been found to
276 preferentially organize with CD59 within the plasma membrane (45). Increased unsaturation of
277 SM results in greater area and decreased lateral diffusion rates of the lipid (46). There was a
278 significantly higher percentage of SM(36:2) (36 acyl carbons, 2 total double bonds) in CD59 KO
279 compared to WT cells. The increased unsaturation within the SM 36C species may result in less
280 ordered membrane dynamics, potentially affecting lipid raft organization and ability to coalesce
281 in a perinuclear locale after bacterial contact (Figure 5). CD59 KO also altered flux through
282 several lipid biosynthesis and catabolic pathways with similar directionality across two
283 independent experiments (Figure 6E). Altogether, this indicates that the absence of CD59 alters
284 the homeostatic maintenance of lipid species composition in the host cell.
285
286

287 **Discussion**

288 In this work we demonstrated that optimal function of the *Yersinia pseudotuberculosis*
289 T3SS requires host cell CD59. While depletion of host CD59 did not eliminate the ability of *Yptb*
290 to form pores and translocate effector Yop substrates into target cells, a marked reduction in
291 T3SS function was observed. This result indicates that CD59 is unlikely to function as a receptor
292 for the T3SS machinery. Consistent with an indirect role in supporting T3SS function, the release
293 of all surface-exposed GPI-linked proteins prior to infection did not reduce *Yptb*(Δ5)-dependent
294 pore formation. These data, together with the inability of the CD59-binding protein ILY^{PP} to
295 block the T3SS machinery, collectively indicate that CD59 is unlikely to directly interact with
296 pathogen components.

297 Host focal adhesion complexes formed upon *Yersinia* engagement with integrins are
298 important sites of signal transduction that are targeted by the tyrosine phosphatase YopH, which
299 disassembles them and helps prevent phagocytosis of bacteria. We found that CD59 facilitates
300 efficient focal adhesion disruption by *Yptb* (Figure 4). In contrast, CD59 depletion increased the
301 average FA size, resulting in a greater total FA area per infected cell. Since translocation is
302 decreased in the absence of CD59, there may be less YopH available to cause focal adhesion
303 disassembly. Alternatively, CD59 has been shown to play a role in several signal transduction
304 pathways, including the activation of Src-family kinases such as Lyn, Fyn, and Lck, some of
305 which are known to interact with FAK (18, 40, 47). CD59 could be involved in activating or
306 recruiting these components to the site of bacterial binding, so that in its absence, these pathways
307 are muted or less accessible to the Yops. Lipid raft domains, of which CD59 is a hallmark
308 component, are also recruited and involved in integrin clustering and likely promote the
309 assembly and reinforcement of FAs (34). CD59 effects on trafficking may not be limited to host

310 cell components, as its loss may interfere with Yop localization, preventing access to signaling
311 structures normally targeted by the Yops.
312 A series of studies indicates that the T3SS translocation complex may interact with lipid
313 raft components. In our previous study, CCR5 was identified as important for T3SS function.
314 CCR5 is in the same family of G protein-coupled receptors (GPCRs) as Fpr1, a recently
315 identified receptor for *Yersinia pestis* that is not required for *Yptb* T3SS function (17, 48). That
316 CCR5 depletion did not completely abolish translocation of *Yptb* T3SS effectors is consistent
317 with *Yptb* targeting functionally redundant receptors, in contrast to the profound importance of
318 Fpr1 for *Y. pestis*. Interestingly, chemokine receptors are known to colocalize with membrane
319 raft markers such as GM1 (49). A similar T3SS-wielding pathogen, *Pseudomonas aeruginosa*,
320 was found to preferentially bind the host receptor glycosphingolipid globotriaosylceramide
321 (Gb3), and depletion of either flotillin or CD59, both found in raft nanodomains with Gb3,
322 reduced uptake of *P. aeruginosa* (50). Functional lipid rafts are important for adhesion and T3SS
323 function in *Shigella*, EPEC, and *Salmonella* as well (25-27). These findings indicate that the
324 organization of various host proteins into structured membrane regions may provide the most
325 efficient target for *Yersinia* to dock, form pores, and deliver Yops via the T3SS.
326 We examined whether CD59 affected ganglioside-rich domains by fluorescently labeling
327 the raft marker GM1. In uninfected cells, the GM1 marker was predominantly trafficked to the
328 perinuclear region in the presence of CD59. When CD59 was depleted, there were noticeably
329 more GM1 puncta visible around the cell periphery. This phenotype was markedly enhanced
330 upon infection with WT *Yptb.* Accumulation of the GM1 marker was only detected in the
331 perinuclear region in WT host cells, while this perinuclear localization was completely lost in the
332 absence of CD59 after contact with WT *Yptb*. CD59 may play a role in mobilization of GM1 to

333 the perinuclear region either through endocytosis, plasma membrane rearrangements, or
334 recycling of this marker back to the plasma membrane.
335 When CtxB binds GM1, it is internalized by receptor-mediated endocytosis, and
336 undergoes retrograde trafficking from the plasma membrane through the trans-Golgi network to
337 the ER. This is visualized as perinuclear localization, as we observed in cells with functional
338 CD59 (51). Interestingly, GM1 binding to antibody provokes a different response, with GM1
339 sorting into recycling endosomes followed by release back to the plasma membrane. This is first
340 visualized as the formation of puncta around the cytoplasm, followed by accumulation in
341 pericentriolar recycling endosomes (52, 53). The absence of CD59 may shift how host endocytic
342 pathways are utilized after *Yptb* engagement, favoring a blockade after punta formation. This
343 could result from changes in the plasma membrane that either prevent effective engagement of
344 the T3SS machinery, alter trafficking of bacterial effectors, or prevent hijacking of host factors
345 by bacterial effectors. Obviously, under CD59 depletion conditions, there must be some low-
346 level or improperly functioning activity of the T3SS that exacerbates the inability of the CtxB-
347 engaged GM1 to coalesce in a perinuclear locale in the absence of CD59.
348 The specific lipid composition of the host cell plasma membrane can affect its structure,
349 function, and interactions with pathogens. PC and PE are the two most abundant lipid classes. PC
350 is a cylindrical-shaped lipid that allows tight packing of lipids and is present in higher
351 concentrations along with sphingolipids in the outer leaflet of the plasma membrane (54, 55). PE
352 along with phosphatidylserine (PS) and phosphatidylinositol (PI) are mostly found in the inner
353 leaflet (55). Acyl chain length and degree of saturation are lipid characteristics known to affect
354 plasma membrane stability and fluidity (56). Longer acyl chains tend to increase saturation and
355 result in thicker membranes, which are also more resistant to bending (57). Within the PC lipid

356 species, 34C and 36C (34 and 36 total carbons in total acyl chain content) were the most
357 commonly detected acyl chain totals in our analysis. CD59 KO cells had fewer 34C and 36C
358 total chain contents, while exhibiting an increase in long total acyl chain content (>40) compared
359 to WT cells (Figure 6B). This same trend was found among the PE lipid species, where CD59
360 KO cells had fewer of the most abundant 36C chain contents, and increased very short and very
361 long acyl chain contents (Figure 6C).

362 Acyl chain saturation is also a determinant of plasma membrane organization and fluidity.
363 Fully unsaturated GM1 C16:0 species have been shown previously to co-cluster with CD59,
364 while C16:1 species did not (58). Our analysis showed that SM C36:2 acyl chains were increased
365 in CD59 KO cells compared to WT cells (Figure 6D). The increased levels of unsaturation could
366 have effects on membrane fluidity, raft formation, or lipid-protein interactions. BioPAN analysis
367 revealed altered flux through various catabolic and metabolic pathways, indicating that CD59 is
368 required for proper lipid homeostasis and plasma membrane maintenance (Figure 6E).

369 In this study we have shown that CD59 is required for efficient pore formation and
370 translocation of bacterial effectors via the *Yptb* T3SS. The depletion of CD59 revealed changes in
371 the localization of lipid raft marker GM1 indicating a largescale disruption of membrane
372 dynamics. CD59 is an important structural component of raft domains, and it is possible that
373 when cells lack this abundant GPI-linked protein, the formation, stability, and/or mobility of
374 these domains is disrupted. Disruption may result from deranged lipid signaling or from
375 preventing the interaction of T3SS components with host kinases involved in signal transduction.
376 Future work will focus on determining if other host components involved in lipid raft signaling
377 play critical roles in T3SS function, as well as on identifying the critical step in the T3SS
378 translocator insertion process that requires intact CD59.

379 **Materials and Methods**

380 **Bacterial Strains and Cell Culture Conditions.** All *Y. pseudotuberculosis* strains used
381 are derivatives of YPIII (wildtype) and were generously provided by Joan Mecsas (See Table 1).
382 HEK 293T cells (ATCC) and HeLa cells (ATCC) were maintained in Gibco DMEM + 10% fetal
383 bovine serum and incubated at 37°C, 5% CO_2.

384 Table 1 Bacterial strains used in this study

Background	Strain	Reference
YPIII	YPIIIΔ*yopB* (YPIIIΔB)	(10)
YPIII	YPIIIΔ*yopHMOJE* (YPIIIΔ5)	(10)
YPIII	YPIII E-TEM	(59)
YPIII	YPIII *gfp*+	(60)
YPIII	YPIIIΔ*yopB gfp*+	(60)

385 386 387 388

389 **T3SS induction.** Single colonies of indicated *Yptb* strains were picked from agar plates
390 and grown in 2xYT broth overnight on a rotator at 26°C. Overnight cultures were diluted to A_{600}
391 = 0.200 in induction media (2xYT + 20mM $MgCl_2$ + 20mM $Na_2C_2O_4$), rotated at 26°C for 1.5
392 hours, then moved to 37°C and rotated for 1.5 hours to induce expression of the T3SS prior to all
393 infection assays.

394 **Generation of CRISPR CD59 knockout 293T cells.** Stable monoclonal CD59 KO
395 HEK 293T cells were generated using the LentiCRISPRv2 vector (a gift from Feng Zhang,
396 Addgene plasmid #52961) (28) targeting the 20bp sequence 5' ACGACGTCACAACCCGCTTG
397 3' of the human CD59 coding region. Oligonucleotides containing this targeted region plus 5'
398 BsmBI restriction sites (sense: CACCGACGACGTCACAACCCGCTTG and antisense:
399 AAACCAAGCGGGTTGTGACGTCGTC) were annealed and ligated into the LentiCRISPRv2
400 plasmid at the BsmBI digestion site. The sgRNA-containing vector was linearized within the
401 ampicillin cassette and transfected into WT 293T cells. After 48 hours transfected cells were

402 selected under puromycin and clonal populations were isolated, outgrown, and successful
403 knockout determined using fluorescent antibody labeling and FACS analysis as described below.
404 The same knockout clone was used for all subsequent experiments, including the generation of
405 clonal cell lines with wildtype and high levels of CD59 surface expression.

406 **Generation of CD59 complement and overexpressing 293T cell lines.** 2 x 10^5 WT or
407 CD59 KO HEK 293T cells were seeded in 6-well tissue culture-treated plates and the pcDNA3.1
408 Hygro+ (empty vector) or pcDNA3.1 Hygro+ hCD59 plasmids were transfected using
409 Lipofectamine 2000 (Invitrogen). Hygromycin was added after 48 hours to select for transfected
410 cells, and transfectants were single-cell sorted into 96-well plates containing conditioned cell
411 media. Arising clonal populations were maintained with Hygromycin B to select against loss of
412 the integrated plasmid.

413 **Translocation Assay.** Approximately 2.5 x 10^5 HEK 293T cells were seeded in tissue
414 culture- treated 24 well dishes overnight. YPIII E-TEM or YPIIIΔ*yopB* E-TEM were grown in
415 induction conditions (See T3SS induction above), diluted in prewarmed DMEM including 10%
416 FBS, and added to 293T cells at an MOI = 1. The infection plates were centrifuged for 5 mins at
417 1000rpm to maximize bacterial contact with cells and incubated at 37°C, 5% CO_2, for 1 hr. Cells
418 were then harvested in 180 µl of PBS. A 10X solution of CCF4-AM reagents was prepared in
419 PBS (LiveBLAzer™ FRET - B/G Loading Kit with CCF4-AM, Invitrogen) (61), 20µL was
420 added to each sample tube, briefly vortexed, and incubated for 20 minutes protected from light at
421 room temperature. Samples were then analyzed on a BD FACS Calibur and data was processed
422 with FlowJo (Tree Star) software, with 10,000 events collected for each sample. Translocation
423 was quantified by subtracting background signal present in uninfected cells and calculating the
424 ratio of the geometric mean fluorescence intensity of the 450/515 channels.

425 **Pore Formation Assay.** Approximately 2.5 x 10^5 HEK 293T cells were seeded in tissue
426 culture-treated 24-well dishes overnight. Overnight bacterial cultures of YPIII Δ*yopHMOJE*
427 (YPIIIΔ5) or YPIIIΔ*yopB* (YPIIIΔB) were grown in T3SS induction conditions prior to infection
428 (See T3SS Induction). Induced YPIIIΔ*yopHMOJE* or YPIIIΔ*yopB* were diluted in prewarmed
429 DMEM + 10% FBS and added to HEK 293T cells at an MOI of 25. After challenge, plates were
430 centrifuged for 5 mins at 200xg and incubated at 37°C, 5% CO_2 for 2 hours. The contents of each
431 well were removed by pipetting the cells up and down, washing with Hanks' balanced salt
432 solution (HBSS), Gibco, resuspending in Live/Dead dye diluted 1:1000 in HBSS
433 (LIVE/DEAD™ Fixable Green Dead Cell Stain Kit, Molecular Probes, Life Technologies), and
434 incubated for 30 minutes protected from light. Cells were washed twice in HBSS containing 1%
435 Bovine Serum Albumin (BSA), resuspended in 0.300mL HBSS, and analyzed by flow cytometry
436 on a BD LSRII flow cytometer. At least 10,000 events were collected per sample. Pore formation
437 was quantified by determining the geometric mean of the FITC channel. Data was processed
438 with FlowJo (Tree Star) software.
439 **CD59 and GPI-linked surface protein detection.** Flow cytometry was utilized to
440 determine the levels of CD59 and GPI-linked proteins on the host cell surface. Live HEK 293Ts
441 cells were washed with PBS, blocked on ice in PBS containing 0.5% BSA for 10 minutes, and
442 pelleted for 5 mins at 300rcf. For CD59 detection, cells were resuspended in mouse anti-human
443 CD59-FITC (BD Pharminogen, clone p282 (H19)), diluted 1:500 in blocking buffer. To detect
444 GPI-linked proteins, cells were resuspended in fluorescently labeled proaerolysin (FLAER,
445 Alexa 488 variant, CedarLane Labs) diluted 1:20 in blocking buffer. Cells were incubated on ice
446 protected from light for 30 minutes, washed once in blocking buffer, resuspended, and
447 transferred to a round bottom polystyrene 12 x 75mm tube for flow cytometry analysis. When

448 fixation was required, cells were washed in PBS, fixed for 20 minutes in PBS containing 4%
449 paraformaldehyde (PFA) at RT, protected from light, washed 3x in PBS, blocked for 1hr in 4%
450 BSA, resuspended in either anti-CD59 or FLAER (1:500 or 1:20, respectively) for 1hr rotating at
451 37°C, washed once, resuspended in blocking buffer, then transferred to round bottom 5mL
452 polystyrene tubes for flow cytometry analysis.

453 **CD59 siRNA knockdown.** HEK 293T or HeLa cells were seeded in 6-well tissue
454 culture-treated plates overnight. 25pmol per well of siGENOME SMARTPOOL human CD59
455 siRNA (Horizon Discovery) or 25pmol of non-targeting control siRNA were transfected using
456 Lipofectamine RNAiMax (Invitrogen). After 48 hours, cells were lifted and seeded in 24-well
457 tissue culture plates. Cells were then challenged with induced YPIII strains after a total of 72
458 hours of siRNA knockdown.

459 **Phospholipase C Treatment.** 5.0 x 10^5 HEK 293T cells per well were seeded into 12-
460 well tissue culture-treated plates overnight. Overnight cultures of YPIII Δ*yopHMOJE* or
461 YPIIIΔ*yopB* were then diluted and induced (see T3SS induction). To cleave surface GPI-linked
462 proteins from HEK 293Ts cells, 0.1U of phospholipase C protein (Phosphatidylinositol-Specific
463 from *Bacillus cereus*, Invitrogen), or an equivalent volume of buffer was added to each well 30
464 minutes prior to infection and incubated at 37°C, 5% CO_2, then cells were infected at MOI = 25.
465 Plates were centrifuged for 5mins at 200xg and incubated at 37°C, 5% CO_2 for 2 hours.
466 Following infection, cells were either assayed for pore formation or probed with FLAER to
467 determine levels of GPI-linked proteins present on the host cell surface.

468 **Expression and purification of intermedilysin proteins.** Plasmid constructs for protein
469 expression of His-tagged WT intermedilysin (His-ILY^{WT}) and a prepore conformation mutant
470 (His-ILY^{PP}) were generously provided by Rodney K. Tweten (62). *E. coli* BL21 (DE3) cultures

471 harboring either the His-ILY^{WT} or His-ILY^{PP} plasmids were grown overnight in LB broth
472 supplemented with 100ug/mL carbenicillin. Overnight cultures were diluted 1:100 in LB and
473 incubated with agitation at 37°C until they reached an A_{600} = 0.8, supplemented with 100ug/mL
474 carbenicillin, and induced by adding 1mM IPTG (final concentration). Cultures were incubated
475 at room temperature overnight and pelleted at 5000rpm for 20 mins at 4°C. Pellets were
476 resuspended in 20mL PBS, 1x EDTA-free cOmplete Protease Inhibitor Cocktail (Sigma), cells
477 were lysed using a microfluidizer (Microfluidics), and the cell lysate centrifuged at 10,000rpm
478 for 30min at 4°C. Cleared lysates were applied to Ni-NTA resin, rotating end over end at 4°C for
479 1hr to allow adsorption, and mixture was transferred to a plastic column. After allowing flow-
480 through of the adsorption mix, the resin was washed with PBS containing steps of 0mM, 20mM,
481 50mM, 80mM, and 120mM imidazole, followed by elution of the protein with PBS containing
482 500mM imidazole, pH =7.2. Protein purity was determined by SDS-PAGE gel and Coomassie
483 staining, and protein concentrations were determined using Bradford reagent (Bio-Rad). Protein
484 was dialyzed overnight into 10mM MES (pH=6.5), 300mM NaCl, 1mM EDTA using dialysis
485 cassettes (Slide-a-Lyzer Cassettes, Thermo), then either stored short-term at 4°C, or long-term by
486 adding 10% glycerol and 5mM DTT before flash freezing for storage at -80°C.

487 **ILY Treatment.** Approximately 5 x 10^5 WT 293T cells were seeded overnight in 12 well
488 plates. To perform inhibitor experiments, cells were pretreated with 100nM ILY^{PP} or an
489 equivalent volume of buffer per well and incubated at 37°C, 5% CO_2 for 1 hr. After pretreatment,
490 cells were challenged with 30nM of ILY^{WT} or buffer, incubated for an additional 2 hours, and
491 assayed for pore formation (See Pore Formation Assay).

492 **Focal Adhesion Immunofluorescence Staining.** HeLa cells were seeded on glass
493 coverslips overnight in 24-well plates. Cells were wash and then challenged at MOI = 5,

494 centrifuged for 5 mins at 200xg, then immediately washed and fixed in 4% PFA. The fixed cells
495 were then washed with 0.05 M Tris buffered saline pH 8.0 (TBS) permeabilized in TBS
496 containing 0.1% Triton X-100 for 2-5 mins and blocked with TBS containing 1% BSA. Cells
497 were incubated with anti-phosphotyrosine, clone 4G10 (EMD Millipore) (1:200 in blocking
498 buffer), washed 3 times, and incubated with donkey anti-mouse IgG-Alexa-Fluor 594 (Jackson
499 ImmunoResearch Laboratories). Coverslips were stained with Hoechst, washed, and mounted
500 with ProLong Glass Antifade (Invitrogen). Images were taken with Zeiss AxioObserver.Z1
501 fluorescent microscope. Focal adhesions were identified and measured in ImageJ using a custom
502 macro that automates various functions to minimize background, increase contrast, and enhance
503 edge detection to identify focal adhesion particles, based on a previously published workflow
504 (41). See Supplementary materials for macro details.

505 **GM1 Immunofluorescence Staining.** HeLa cells were seeded overnight in DMEM
506 containing 10% fetal bovine serum on glass coverslips in 24-well plates. Prior to infection, the
507 culture medium was aspirated and fresh culture medium containing cholera toxin B (CtxB)
508 (Vybrant Lipid Raft Labeling Kit, Molecular Probes) was added. Cells were then infected at MOI
509 = 5 with *Yptb* diluted in DMEM + 10% FBS so that the final concentration of CtxB was 2μg/mL
510 in each well. Plates were placed in centrifuge, subjected to 5min spin at 200xg, then coverslips
511 were washed three times with cold medium, incubated with anti-CtxB at 4°C for 15mins, washed
512 three times with cold PBS, fixed in 4% PBS containing 4% PFA, washed three times in PBS,
513 stained with Hoechst (1:10000) and mounted with ProLong Glass Antifade (Invitrogen).

514 **Lipid Extraction and Data Analysis.** Lipids were extracted from WT and CD59 KO
515 293T cells by the Folch extraction method (44) as follows. CD59 KO and WT 293T cells were
516 grown in DMEM + 10% FBS until ~80% confluency in one 10cm plate per sample replicate, and

517 medium was changed 2 hours prior to harvesting. Cells were rinsed with PBS, lifted with 0.05%
518 trypsin, spun down for 5min at 200xg, washed with PBS, and resuspended with PBS in a total
519 volume of 200µL. Cells were transferred to glass vials and 2:1 chloroform: methanol was added
520 to a final volume of 4mL. Samples were then agitated for 30 min on an orbital shaker at RT
521 before 800µL water was added, vortexed 1 min, and allowed to stand for 10 minutes before
522 centrifuging for 5min at 1000xg to separate into three phases. The lower phase containing
523 nonpolar lipids was carefully transferred with a glass pipette from the vial into the microtube,
524 then evaporated under nitrogen and stored at -80 °C. Samples were then analyzed via high-
525 resolution LC-MS/MS, and the lipids were identified and quantified with LipidSearch software
526 by the BIDMC-Harvard Mass Spectrometry Facility according to their published protocol
527 (special thanks to Dr. John Asara, Director) (44). Lipid peak data were` normalized by percent
528 abundance within each sample. PCA analysis was performed using MetaboAnalyst 5.0. Lipid
529 pathway analysis performed using LIPIDMAPS BioPan software.

530
531
532
533 **Acknowledgements**

534 We would like to acknowledge Stephen Kwok and Alan Parmelee from the Tufts Flow
535 Cytometry Core Facility for assistance in flow cytometry, Dr. Joan Mecsas and her lab for
536 *Yersinia* strains and discussions, as well as Drs. Marta Gaglia and Katya Heldwein for
537 experimental suggestions. We thank Drs. Kevin Manera, Atish RoyChowdhury and Bixi He for
538 critical review of the manuscript. This work was supported by NIAID awards R21AI085250,
539 and R01AI110684 to R.R.I. KJD was supported by a NIAID Training Grant T32AI007422.

540

541

542 **Author Contributions**

543 Kristen Davis, Conceptualized and designed the analysis, collected, analyzed, and interpreted the
544 data, writing of original draft, editing of the paper; Kerri Sheahan, conceptualization, constructed
545 CD59 KO cell line, collected preliminary data; Connor Murphy, conceptualization, collected
546 preliminary data; Ralph Isberg, conceptualization and design of analysis, funding acquisition,
547 project administration, methodology, interpretation of data, editing and review of manuscript.

548

549

550

551 1. Dewoody RS, Merritt PM, Marketon MM. 2013. Regulation of the Yersinia type III
552 secretion system: traffic control. Front Cell Infect Microbiol 3:4.
553 2. Cornelis GR. 2006. The type III secretion injectisome. Nat Rev Microbiol 4:811-25.
554 3. Bliska JB, Wang X, Viboud GI, Brodsky IE. 2013. Modulation of innate immune
555 responses by Yersinia type III secretion system translocators and effectors. Cell Microbiol
556 15:1622-31.
557 4. Cornelis GR, Boland A, Boyd AP, Geuijen C, Iriarte M, Neyt C, Sory MP, Stainier I.
558 1998. The virulence plasmid of Yersinia, an antihost genome. Microbiol Mol Biol Rev
559 62:1315-52.
560 5. Portnoy DA, Falkow S. 1981. Virulence-associated plasmids from Yersinia enterocolitica
561 and Yersinia pestis. J Bacteriol 148:877-83.
562 6. Gemski P, Lazere JR, Casey T, Wohlhieter JA. 1980. Presence of a virulence-associated
563 plasmid in Yersinia pseudotuberculosis. Infect Immun 28:1044-7.
564 7. Matteï PJ, Faudry E, Job V, Izoré T, Attree I, Dessen A. 2011. Membrane targeting and
565 pore formation by the type III secretion system translocon. FEBS J 278:414-26.
566 8. Viboud GI, Mejía E, Bliska JB. 2006. Comparison of YopE and YopT activities in
567 counteracting host signalling responses to Yersinia pseudotuberculosis infection. Cell
568 Microbiol 8:1504-15.
569 9. Aepfelbacher M, Trasak C, Wilharm G, Wiedemann A, Trulzsch K, Krauss K, Gierschik
570 P, Heesemann J. 2003. Characterization of YopT effects on Rho GTPases in Yersinia
571 enterocolitica-infected cells. J Biol Chem 278:33217-23.
572 10. Logsdon LK, Mecsas J. 2003. Requirement of the Yersinia pseudotuberculosis effectors
573 YopH and YopE in colonization and persistence in intestinal and lymph tissues. Infect
574 Immun 71:4595-607.
575 11. Black DS, Bliska JB. 2000. The RhoGAP activity of the Yersinia pseudotuberculosis
576 cytotoxin YopE is required for antiphagocytic function and virulence. Mol Microbiol
577 37:515-27.
578 12. von Pawel-Rammingen U, Telepnev M, Schmidt G, Aktories K, Wolf-Watz H, Rosqvist
579 R. 2000. GAP activity of the Yersinia YopE cytotoxin specifically targets the Rho
580 pathway: a mechanism for disruption of actin microfilament structure. Molecular
581 Microbiology 36:737-748.
582 13. Mejía E, Bliska JB, Viboud GI. 2008. Yersinia controls type III effector delivery into host
583 cells by modulating Rho activity. PLoS Pathog 4:e3.
584 14. Blondel CJ, Park JS, Hubbard TP, Pacheco AR, Kuehl CJ, Walsh MJ, Davis BM, Gewurz
585 BE, Doench JG, Waldor MK. 2016. CRISPR/Cas9 Screens Reveal Requirements for Host
586 Cell Sulfation and Fucosylation in Bacterial Type III Secretion System-Mediated
587 Cytotoxicity. Cell Host Microbe 20:226-37.
588 15. Deruelle V, Bouillot S, Job V, Taillebourg E, Fauvarque MO, Attree I, Huber P. 2021. The
589 bacterial toxin ExoU requires a host trafficking chaperone for transportation and to
590 induce necrosis. Nat Commun 12:4024.
591 16. Swimm AI, Kalman D. 2008. Cytosolic extract induces Tir translocation and pedestals in
592 EPEC-infected red blood cells. PLoS Pathog 4:e4.
593 17. Sheahan KL, Isberg RR. 2015. Identification of mammalian proteins that collaborate with
594 type III secretion system function: involvement of a chemokine receptor in supporting
595 translocon activity. MBio 6:e02023-14.

596 18. Kimberley FC, Sivasankar B, Paul Morgan B. 2007. Alternative roles for CD59. Mol
597 Immunol 44:73-81.
598 19. Sugita Y, Nakano Y, Tomita M. 1988. Isolation from human erythrocytes of a new
599 membrane protein which inhibits the formation of complement transmembrane channels.
600 J Biochem 104:633-7.
601 20. Holguin MH, Fredrick LR, Bernshaw NJ, Wilcox LA, Parker CJ. 1989. Isolation and
602 characterization of a membrane protein from normal human erythrocytes that inhibits
603 reactive lysis of the erythrocytes of paroxysmal nocturnal hemoglobinuria. J Clin Invest
604 84:7-17.
605 21. Rollins SA, Sims PJ. 1990. The complement-inhibitory activity of CD59 resides in its
606 capacity to block incorporation of C9 into membrane C5b-9. J Immunol 144:3478-83.
607 22. Giddings KS, Zhao J, Sims PJ, Tweten RK. 2004. Human CD59 is a receptor for the
608 cholesterol-dependent cytolysin intermedilysin. Nat Struct Mol Biol 11:1173-8.
609 23. Farrand AJ, Hotze EM, Sato TK, Wade KR, Wimley WC, Johnson AE, Tweten RK. 2015.
610 The Cholesterol-dependent Cytolysin Membrane-binding Interface Discriminates Lipid
611 Environments of Cholesterol to Support beta-Barrel Pore Insertion. J Biol Chem
612 290:17733-17744.
613 24. Simons K, Ehehalt R. 2002. Cholesterol, lipid rafts, and disease. J Clin Invest 110:597-
614 603.
615 25. Hayward RD, Cain RJ, McGhie EJ, Phillips N, Garner MJ, Koronakis V. 2005.
616 Cholesterol binding by the bacterial type III translocon is essential for virulence effector
617 delivery into mammalian cells. Mol Microbiol 56:590-603.
618 26. van der Goot FG, Tran van Nhieu G, Allaoui A, Sansonetti P, Lafont F. 2004. Rafts can
619 trigger contact-mediated secretion of bacterial effectors via a lipid-based mechanism. J
620 Biol Chem 279:47792-8.
621 27. Lafont F, van der Goot FG. 2005. Bacterial invasion via lipid rafts. Cell Microbiol 7:613-
622 20.
623 28. Sanjana NE, Shalem O, Zhang F. 2014. Improved vectors and genome-wide libraries for
624 CRISPR screening. Nat Methods 11:783-784.
625 29. Viboud GI, Bliska JB. 2005. Yersinia outer proteins: role in modulation of host cell
626 signaling responses and pathogenesis. Annu Rev Microbiol 59:69-89.
627 30. Harmon DE, Davis AJ, Castillo C, Mecsas J. 2010. Identification and characterization of
628 small-molecule inhibitors of Yop translocation in Yersinia pseudotuberculosis.
629 Antimicrob Agents Chemother 54:3241-54.
630 31. Soltani CE, Hotze EM, Johnson AE, Tweten RK. 2007. Specific protein-membrane
631 contacts are required for prepore and pore assembly by a cholesterol-dependent cytolysin.
632 J Biol Chem 282:15709-16.
633 32. Guignot J, Tran Van Nhieu G. 2016. Bacterial Control of Pores Induced by the Type III
634 Secretion System: Mind the Gap. Front Immunol 7:84.
635 33. Knodler LA, Celli J, Finlay BB. 2001. Pathogenic trickery: deception of host cell
636 processes. Nat Rev Mol Cell Biol 2:578-88.
637 34. Fuentes DE, Butler PJ. 2012. Coordinated Mechanosensitivity of Membrane Rafts and
638 Focal Adhesions. Cell Mol Bioeng 5:143-154.
639 35. Black DS, Montagna LG, Zitsmann S, Bliska JB. 1998. Identification of an amino-
640 terminal substrate-binding domain in the Yersinia tyrosine phosphatase that is required
641 for efficient recognition of focal adhesion targets. Mol Microbiol 29:1263-74.

642 36. Rolán HG, Durand EA, Mecsas J. 2013. Identifying Yersinia YopH-targeted signal
643 transduction pathways that impair neutrophil responses during in vivo murine infection.
644 Cell Host Microbe 14:306-17.
645 37. Andersson K, Carballeira N, Magnusson KE, Persson C, Stendahl O, Wolf-Watz H,
646 Fällman M. 1996. YopH of Yersinia pseudotuberculosis interrupts early phosphotyrosine
647 signalling associated with phagocytosis. Mol Microbiol 20:1057-69.
648 38. Persson C, Carballeira N, Wolf-Watz H, Fällman M. 1997. The PTPase YopH inhibits
649 uptake of Yersinia, tyrosine phosphorylation of p130Cas and FAK, and the associated
650 accumulation of these proteins in peripheral focal adhesions. EMBO J 16:2307-18.
651 39. Black DS, Bliska JB. 1997. Identification of p130Cas as a substrate of Yersinia YopH
652 (Yop51), a bacterial protein tyrosine phosphatase that translocates into mammalian cells
653 and targets focal adhesions. EMBO J 16:2730-44.
654 40. Lipp AM, Juhasz K, Paar C, Ogris C, Eckerstorfer P, Thuenauer R, Hesse J, Nimmervoll
655 B, Stockinger H, Schütz GJ, Bodenhofer U, Balogi Z, Sonnleitner A. 2014. Lck mediates
656 signal transmission from CD59 to the TCR/CD3 pathway in Jurkat T cells. PLoS One
657 9:e85934.
658 41. Horzum U, Ozdil B, Pesen-Okvur D. 2014. Step-by-step quantitative analysis of focal
659 adhesions. MethodsX 1:56-9.
660 42. Aigal S, Claudinon J, Romer W. 2015. Plasma membrane reorganization: A glycolipid
661 gateway for microbes. Biochim Biophys Acta 1853:858-71.
662 43. Klymchenko AS, Kreder R. 2014. Fluorescent probes for lipid rafts: from model
663 membranes to living cells. Chem Biol 21:97-113.
664 44. Breitkopf SB, Ricoult SJH, Yuan M, Xu Y, Peake DA, Manning BD, Asara JM. 2017. A
665 relative quantitative positive/negative ion switching method for untargeted lipidomics via
666 high resolution LC-MS/MS from any biological source. Metabolomics 13.
667 45. Kinoshita M, Suzuki KG, Matsumori N, Takada M, Ano H, Morigaki K, Abe M, Makino
668 A, Kobayashi T, Hirosawa KM, Fujiwara TK, Kusumi A, Murata M. 2017. Raft-based
669 sphingomyelin interactions revealed by new fluorescent sphingomyelin analogs. J Cell
670 Biol 216:1183-1204.
671 46. Niemela PS, Hyvonen MT, Vattulainen I. 2006. Influence of chain length and
672 unsaturation on sphingomyelin bilayers. Biophys J 90:851-63.
673 47. Wang LN, Gao MH, Wang B, Cong BB, Zhang SC. 2018. A role for GPI-CD59 in
674 promoting T-cell signal transduction via LAT. Oncol Lett 15:4873-4881.
675 48. Osei-Owusu P, Charlton TM, Kim HK, Missiakas D, Schneewind O. 2019. FPR1 is the
676 plague receptor on host immune cells. Nature 574:57-62.
677 49. Popik W, Alce TM, Au WC. 2002. Human immunodeficiency virus type 1 uses lipid raft-
678 colocalized CD4 and chemokine receptors for productive entry into CD4(+) T cells. J
679 Virol 76:4709-22.
680 50. Brandel A, Aigal S, Lagies S, Schlimpert M, Melendez AV, Xu M, Lehmann A, Hummel
681 D, Fisch D, Madl J, Eierhoff T, Kammerer B, Romer W. 2021. The Gb3-enriched
682 CD59/flotillin plasma membrane domain regulates host cell invasion by Pseudomonas
683 aeruginosa. Cell Mol Life Sci 78:3637-3656.
684 51. Chinnapen DJ, Chinnapen H, Saslowsky D, Lencer WI. 2007. Rafting with cholera toxin:
685 endocytosis and trafficking from plasma membrane to ER. FEMS Microbiol Lett
686 266:129-37.

687 52. Iglesias-Bartolome R, Trenchi A, Comin R, Moyano AL, Nores GA, Daniotti JL. 2009.
688 Differential endocytic trafficking of neuropathy-associated antibodies to GM1
689 ganglioside and cholera toxin in epithelial and neural cells. Biochim Biophys Acta
690 1788:2526-40.
691 53. Cai B, Xie S, Liu F, Simone LC, Caplan S, Qin X, Naslavsky N. 2014. Rapid degradation
692 of the complement regulator, CD59, by a novel inhibitor. J Biol Chem 289:12109-12125.
693 54. Torres M, Parets S, Fernandez-Diaz J, Beteta-Gobel R, Rodriguez-Lorca R, Roman R,
694 Llado V, Rossello CA, Fernandez-Garcia P, Escriba PV. 2021. Lipids in Pathophysiology
695 and Development of the Membrane Lipid Therapy: New Bioactive Lipids. Membranes
696 (Basel) 11.
697 55. Skotland T, Kavaliauskiene S, Sandvig K. 2020. The role of lipid species in membranes
698 and cancer-related changes. Cancer Metastasis Rev 39:343-360.
699 56. Vanni S, Riccardi L, Palermo G, De Vivo M. 2019. Structure and Dynamics of the Acyl
700 Chains in the Membrane Trafficking and Enzymatic Processing of Lipids. Acc Chem Res
701 52:3087-3096.
702 57. Rawicz W, Olbrich KC, McIntosh T, Needham D, Evans E. 2000. Effect of chain length
703 and unsaturation on elasticity of lipid bilayers. Biophys J 79:328-39.
704 58. Arumugam S, Schmieder S, Pezeshkian W, Becken U, Wunder C, Chinnapen D, Ipsen
705 JH, Kenworthy AK, Lencer W, Mayor S, Johannes L. 2021. Ceramide structure dictates
706 glycosphingolipid nanodomain assembly and function. Nat Commun 12:3675.
707 59. Maldonado-Arocho FJ, Green C, Fisher ML, Paczosa MK, Mecsas J. 2013. Adhesins and
708 host serum factors drive Yop translocation by yersinia into professional phagocytes
709 during animal infection. PLoS Pathog 9:e1003415.
710 60. Crimmins GT, Mohammadi S, Green ER, Bergman MA, Isberg RR, Mecsas J. 2012.
711 Identification of MrtAB, an ABC transporter specifically required for Yersinia
712 pseudotuberculosis to colonize the mesenteric lymph nodes. PLoS Pathog 8:e1002828.
713 61. Nguyen GT, McCabe AL, Fasciano AC, Mecsas J. 2019. Detection of Cells Translocated
714 with Yersinia Yops in Infected Tissues Using β-Lactamase Fusions. Methods Mol Biol
715 2010:117-139.
716 62. LaChapelle S, Tweten RK, Hotze EM. 2009. Intermedilysin-receptor interactions during
717 assembly of the pore complex: assembly intermediates increase host cell susceptibility to
718 complement-mediated lysis. J Biol Chem 284:12719-26.
719 63. Gaud C, B CS, Nguyen A, Fedorova M, Ni Z, O'Donnell VB, Wakelam MJO, Andrews S,
720 Lopez-Clavijo AF. 2021. BioPAN: a web-based tool to explore mammalian lipidome
721 metabolic pathways on LIPID MAPS. F1000Res 10:4.
722

723

724 **FIGURE LEGENDS**

725 **Figure 1. Knockout and increased surface levels of host cell CD59 result in inefficient pore**
726 **formation when challenged by *Yptb*.** (**A)** WT and CD59 KO HEK 293T cells were probed with
727 FITC-conjugated α-human CD59 and analyzed by flow cytometry to quantitate cell surface
728 CD59. Histogram displays total counts for fluorescence of FITC channel, collecting 10,000
729 events per sample. **(B)** HEK 293T cells were challenged with YPIIIΔ*yopHMOJE* (YPIIIΔ5) or
730 YPIII*yopB* (YPIIIΔB) at MOI = 25 for 2 hours. Cells were labeled with FITC LIVE/DEAD stain
731 and analyzed by flow cytometry to determine extent of pore formation (Materials and Methods).
732 **(C)** CD59 KO 293T cells were transfected with a plasmid expressing human CD59 and stable
733 monoclonal cell lines were obtained with CD59 levels that were similar to endogenously
734 expressed protein (WT1 and WT2) or which were overexpressed (OE1 and OE2). The histogram
735 indicates the level of FITC-conjugated α-human CD59 labeling for the WT, CD59 KO, and
736 pCD59 clones as determined by flow cytometry. **(D)** Indicated cell lines were challenged at MOI
737 = 25 for 2 hrs with YPIIIΔ5 (See Supplemental Figure S1 for YPIIIΔB control). Cells were
738 labeled with FITC LIVE/DEAD stain and analyzed by flow cytometry to determine extent of
739 pore formation. Data are geometric mean ± SEM of the fluorescence intensity normalized to WT.
740 Results represent three independent experiments performed in technical triplicate. Statistical
741 significance was calculated using a one-way ANOVA with Dunnett's multiple comparison test
742 (*$p < 0.05$).

743

744

745 **Figure 2. Knockdown of host cell CD59 inhibits translocation of T3SS substrates during**
746 ***Yptb* infection.** WT 293T cells were transfected with either human CD59 siRNA or non-
747 targeting control siRNA to knock down CD59 expression. Assays were performed after 72 total
748 hours of transfection. **(A)** Cells were probed with FITC-conjugated α-human CD59 and analyzed
749 by flow cytometry for cell surface localization of CD59. **(B, C)** Approximately 2.5 x 10^5 siRNA
750 transfected cells were seeded overnight. Cells were challenged with YPIII/YopE-TEM or
751 YPIIIΔ*yopB*/YopE-TEM at MOI = 1 for 1 hour. Infected cells were harvested, loaded with
752 CCF4-AM and analyzed by flow cytometry. **(B)** Contour plots displaying the fluorescence
753 intensity of the blue channel (450nm) indicative of YopE translocation vs. the green channel
754 (515nm) displaying all cells. **(C)** Translocation was calculated by determining the ratio of the
755 geometric MFI for the 450/515 channels. Data shown are a representative experiment (from 3
756 independent experiments performed in technical triplicate).

757

758 **Figure 3. Host cell CD59 indirectly supports YPIII T3SS-dependent pore formation. (A,B)**
759 ILY^{PP} treatment effectively blocks binding and subsequent pore formation by ILY^{WT}. WT 293T
760 cells were seeded overnight in 12 well plates. Cells were pretreated with 100nM of ILY^{PP} or
761 buffer for 1 hour, challenged with either 30nM ILY^{WT} **(A)** or YPIIIΔ5 or YPIIIΔB at MOI=25 **(B)**
762 and incubated for 2 hours. Cells were harvested and assayed for pore formation. Results shown
763 in panels A and B represent data from three independent experiments in technical duplicate or
764 triplicate and all pore formation data was normalized to untreated 293T cells challenged by
765 YPIIIΔ5. **(C)** WT HEK 293T cells were seeded overnight in 12-well plates. Cells were treated
766 with phospholipase C (PLC) and incubated at 37°C, 5% CO_2 for 30 mins before harvesting and

767 labeling with FLAER for detection of GPI-linked proteins by flow cytometry. **(D)** WT HEK
768 293T cells were seeded overnight in 12-well plates and pretreated with PLC or buffer prior to
769 challenge with YPIIIΔ5 or YPIIIΔB at MOI = 25 for 2 hrs. Cells were then harvested and
770 assayed for pore formation. Data are geometric means ± SEM of MFI after subtraction of
771 uninfected control cell background and normalized to untreated 293T cells challenged by
772 YPIIIΔ5. Results represent three independent experiments done in technical duplicate or
773 triplicate. Statistical significance was calculated using an unpaired two-tailed Welch's t test (*p <
774 0.05).
775
776 **Figure 4. CD59 depletion lowers focal adhesion disruption by *Yptb*.** HeLa cells were
777 transfected with either siCD59 or the siNT control for 72 hours. Cells were challenged with *Yptb*
778 *gfp*+ at an MOI = 5 by 5 min centrifugation at 200xg followed by immediate washing and fixing.
779 The cells were then immunostained with anti-pTyr followed by probing with anti-mouse-AF594,
780 and nuclei were stained with Hoechst (1:10000). **(A)** Focal adhesion staining with pTyr of
781 uninfected cells. **(B)** Cells challenged with *Yptb gfp*+. Scale bar = 10um. Focal adhesions were
782 identified and measured as described (Materials and Methods). **(C, D)** Average size and total area
783 displayed. Data analyzed using Ordinary One Way ANOVA followed by Sidak's test (*p < 0.05).
784
785 **Figure 5. CD59 knockdown affects localization of the lipid raft marker GM1.** HeLa cells
786 were transfected for 72 hrs with 25nM of siCD59 or non-targeting siRNA, then seeded on glass
787 coverslips for 24hrs prior to bacterial challenge. **(A, B)** Uninfected. **(C,D)** Cells challenged with
788 YPIIIΔB(pGFP). **(E,F)** Cells challenged with YPIII-WT(pGFP). Infections were performed at
789 MOI = 5 in presence of CtxB-AlexaFluor594. Bacterial-host cell contact was initiated by 5 min

790 centrifugation at 200xg followed by immediate washing and incubation with α-Ctx. Cells were
791 fixed with 4% PFA, and nuclei stained with Hoechst (1:10000). Scale bar = 10μm
792
793 **Figure 6. CD59 KO alters cellular lipid composition.** Lipids were extracted from HEK 293T
794 WT and CD59 KO cells (Materials and Methods). Representative results of two independent
795 experiments performed in triplicate. **(A)** Knockout of CD59 alters lipid profile. Principal
796 component analysis (PCA) of CD59 KO vs WT cells. Data was normalized by percent
797 abundance within each sample. **(B)** Sum of carbon counts of PC acyl species as a percentage of
798 total PC within each sample. **(C)** Sum of carbon counts of PE acyl species as a percentage of
799 total PE within each sample. **(D)** Saturation levels of SM lipid species as a percentage of total
800 SM within each sample. Significance determined by unpaired t test using two-stage step-up with
801 FDR of 1% for multiple comparisons. **(E)** Alteration of lipid flux as a consequence of loss of
802 CD59. Lipid peak data normalized by percent abundance was analyzed using LIPIDMAPS
803 BioPan software, available through LIPIDMAPS.org (63). Lipid subclass pathways displayed
804 were found to be similarly altered in both experiments.
805
806 **Figure S1. Pore formation by *Yptb* is T3SS-dependent.** CD59KO HEK 293T cells were
807 transfected with a plasmid expressing human CD59, and stable monoclonal cell lines were
808 obtained with CD59 levels that were similar to endogenously expressed protein (WT1 and WT2)
809 or which were overexpressed (OE1 and OE2). Indicated cell lines were challenged with
810 YPIIIΔ*yopHMOJE* (YPIIIΔ5) or YPIIIΔ*yopB* (YPIIIΔB) at MOI = 25 for 2 hrs. Cells were
811 labeled with FITC LIVE/DEAD stain and analyzed by flow cytometry to determine extent of

812 pore formation. Data are geometric mean ± SEM of the fluorescence intensity normalized to WT.

813 Data shown is representative of three individual experiments.

814

815 **Figure S2.** CD59 knockdown does not change surface levels of GM. **(A, B)** siNT control cells

816 and siCD59 knockdown cells were probed with FITC-conjugated α-human CD59 **(A)** or

817 immunolabeled for GM1 **(B)** and analyzed by flow cytometry after a 72 hr knockdown.

818

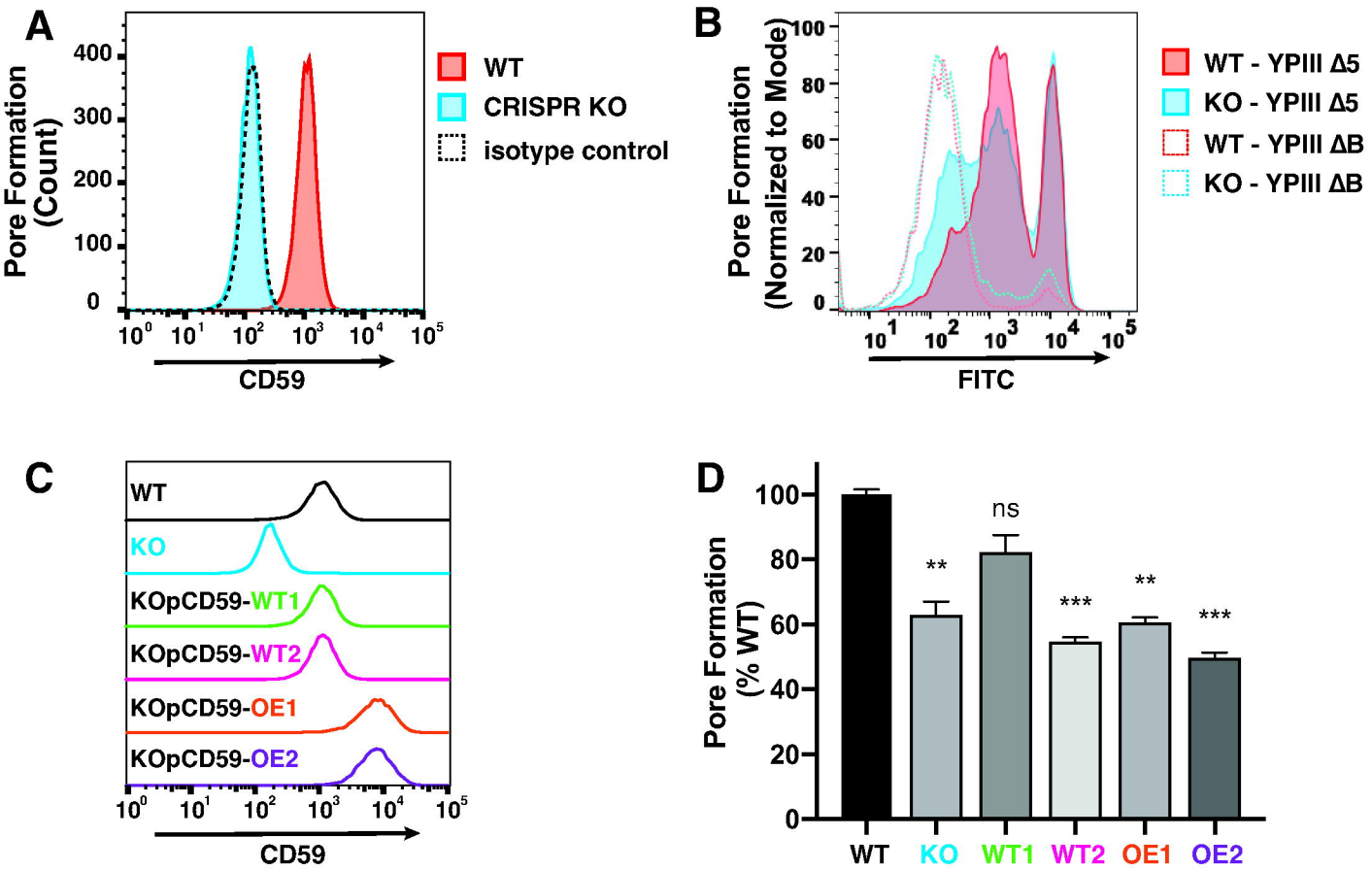
A
Pore Formation (Count)
400
300
200
100
0
10^0 10^1 10^2 10^3 10^4 10^5
CD59
WT
CRISPR KO
isotype control
B
Pore Formation (Normalized to Mode)
100
80
60
40
20
0
10^1 10^2 10^3 10^4 10^5
FITC
WT - YPIII Δ5
KO - YPIII Δ5
WT - YPIII ΔB
KO - YPIII ΔB
C
WT
KO
KOpCD59-WT1
KOpCD59-WT2
KOpCD59-OE1
KOpCD59-OE2
10^0 10^1 10^2 10^3 10^4 10^5
CD59
D
Pore Formation (% WT)
100
80
60
40
20
0
ns
**
***
**
***
WT
KO
WT1
WT2
OE1
OE2

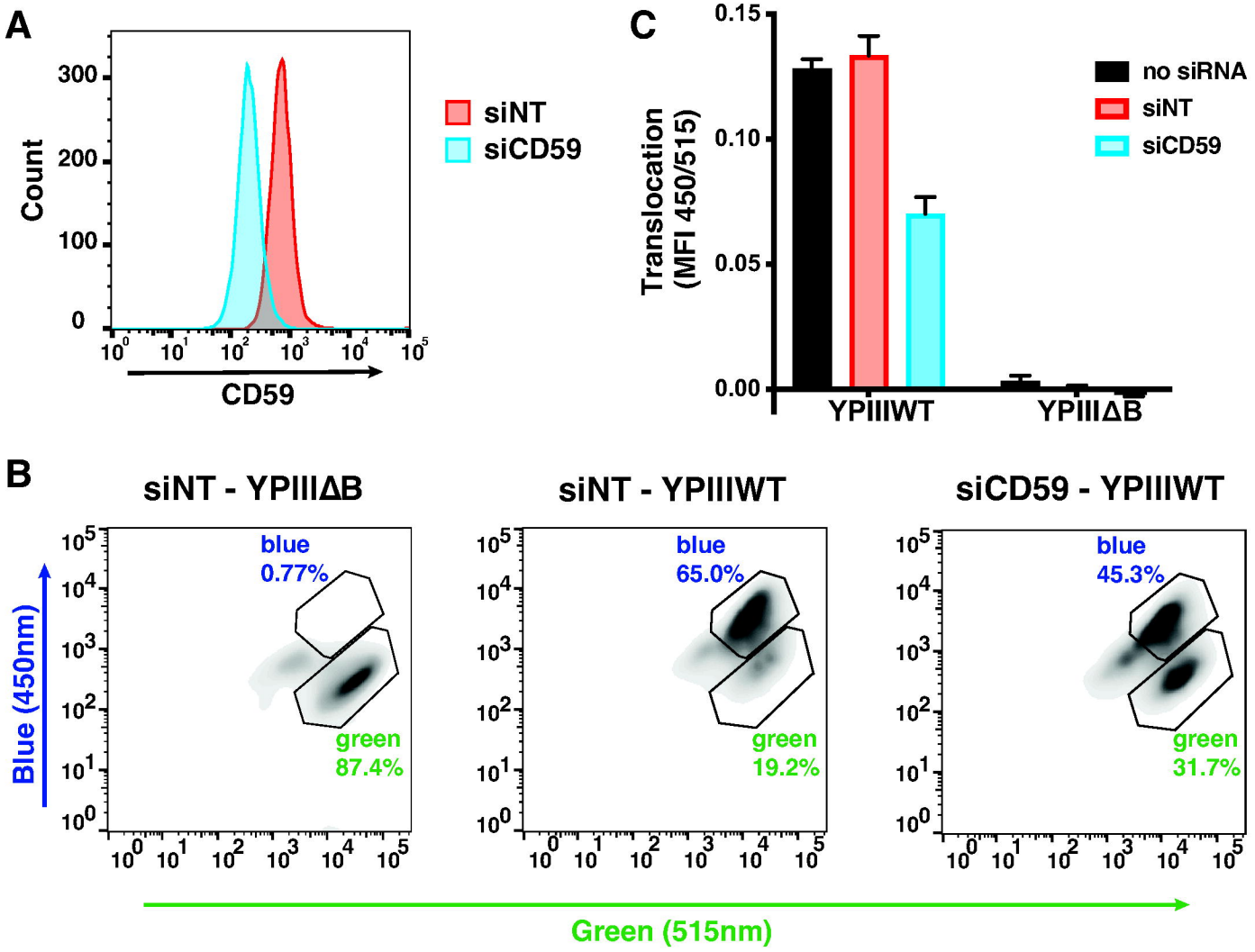
A
Count
300
200
100
0
CD59
siNT
siCD59
C
Translocation (MFI 450/515)
0.15
0.10
0.05
0.00
no siRNA
siNT
siCD59
YPIIIWT
YPIIIΔB
B
siNT - YPIIIΔB
siNT - YPIIIWT
siCD59 - YPIIIWT
blue
0.77%
green
87.4%
blue
65.0%
green
19.2%
blue
45.3%
green
31.7%
Blue (450nm)
Green (515nm)

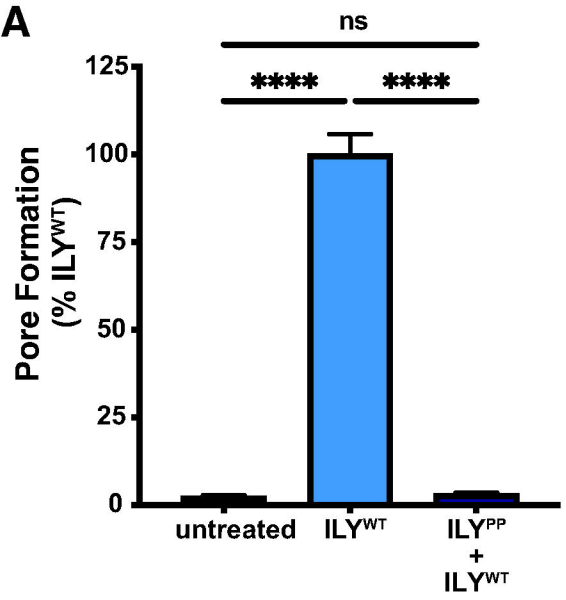
A
ns
****
****
125
100
75
50
25
0
Pore Formation
(% ILY^WT)
untreated
ILY^WT
ILY^PP
+
ILY^WT

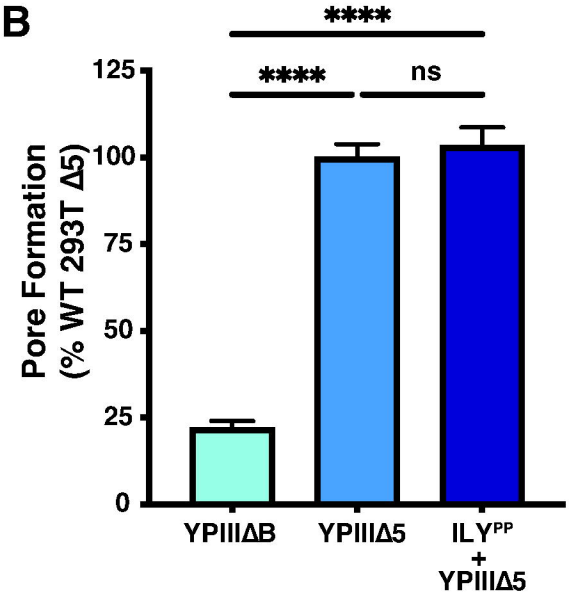
B
****
****
ns
125
100
75
50
25
0
Pore Formation
(% WT 293T Δ5)
YPIIIΔB
YPIIIΔ5
ILY^PP
+
YPIIIΔ5

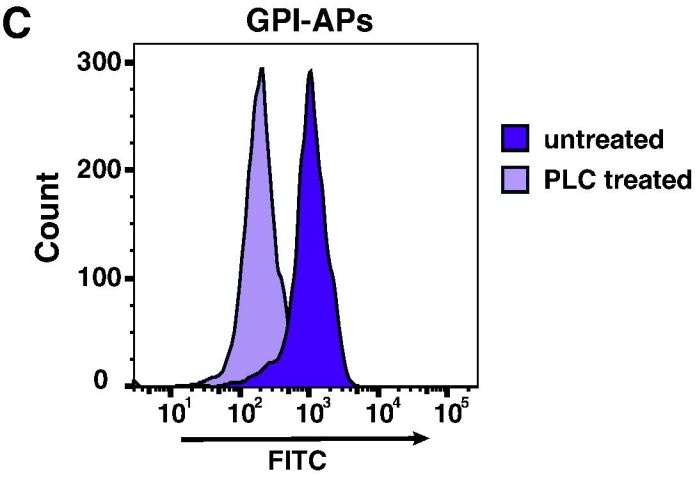
C
GPI-APs
300
200
100
0
Count
10^1
10^2
10^3
10^4
10^5
FITC
untreated
PLC treated

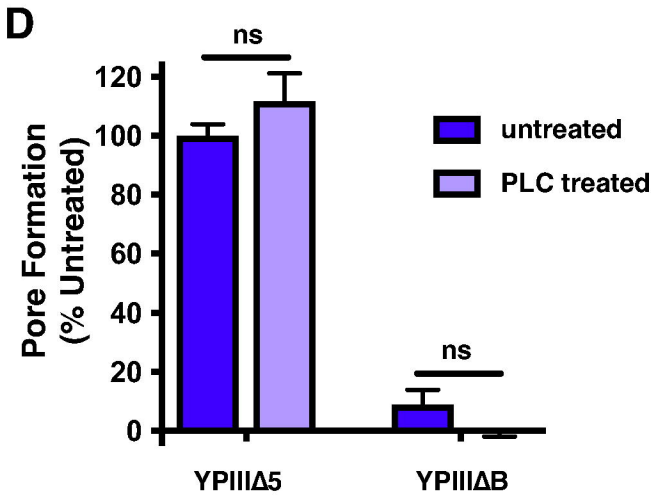
D
ns
ns
120
100
80
60
40
20
0
Pore Formation
(% Untreated)
untreated
PLC treated
YPIIIΔ5
YPIIIΔB

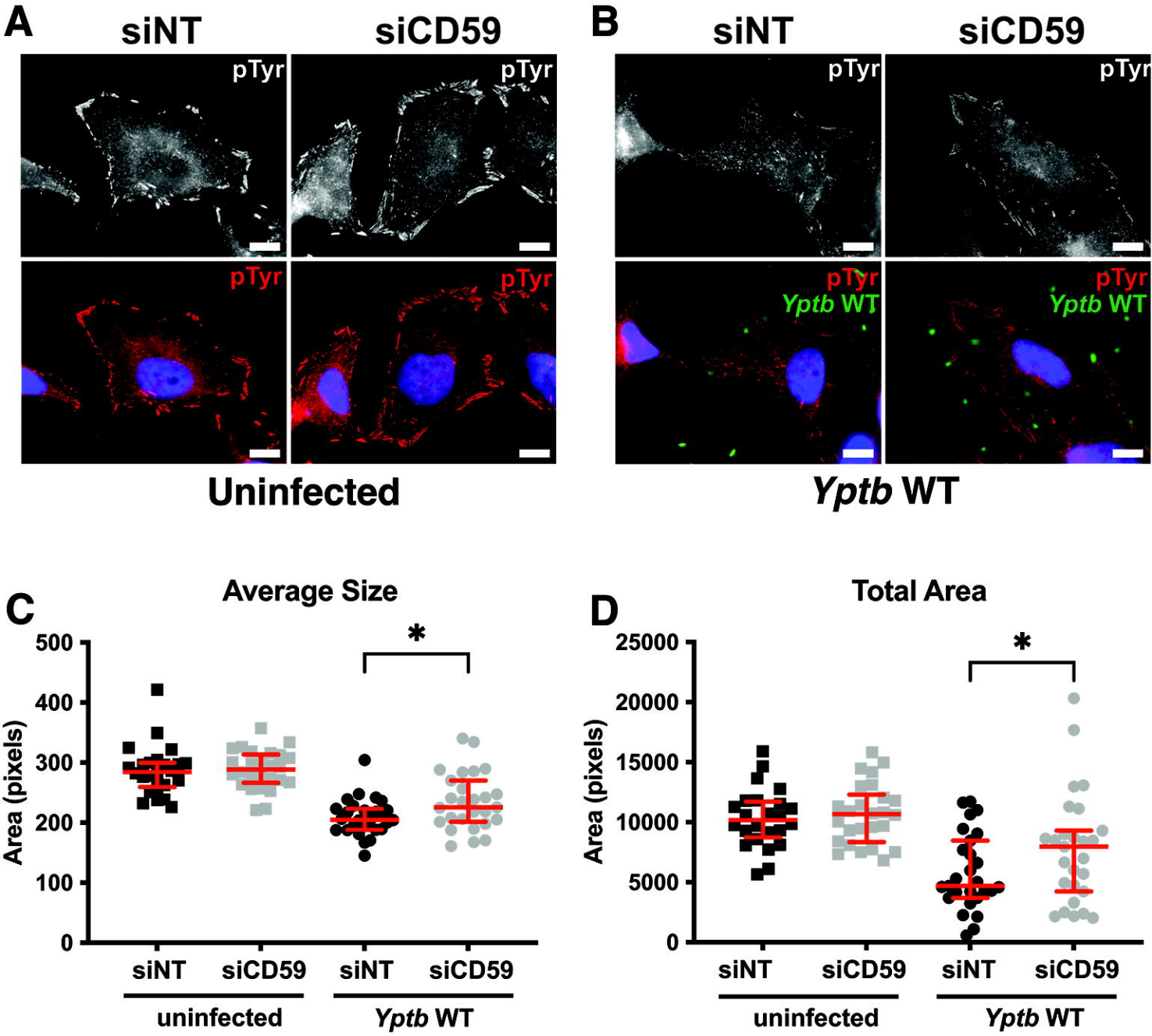
A
siNT
siCD59
pTyr
pTyr
pTyr
pTyr
Uninfected
B
siNT
siCD59
pTyr
pTyr
pTyr
Yptb WT
pTyr
Yptb WT
Yptb WT
C
Average Size
Area (pixels)
500
400
300
200
100
0
*
siNT
siCD59
siNT
siCD59
uninfected
Yptb WT
D
Total Area
Area (pixels)
25000
20000
15000
10000
5000
0
*
siNT
siCD59
siNT
siCD59
uninfected
Yptb WT

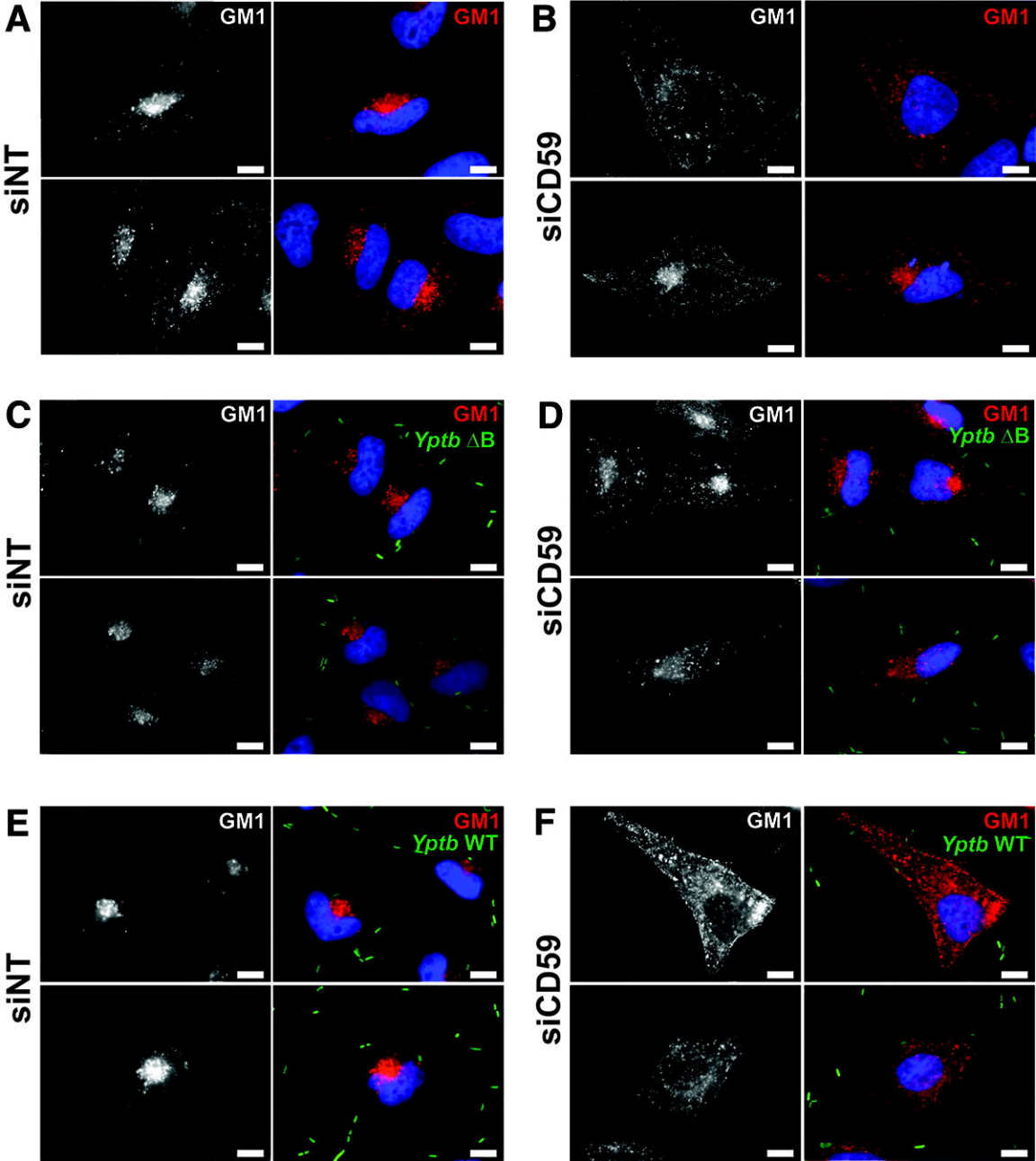
A
GM1
GM1
siNT
B
GM1
GM1
siCD59
C
GM1
GM1
Yptb ΔB
siNT
D
GM1
GM1
Yptb ΔB
siCD59
E
GM1
GM1
Yptb WT
siNT
F
GM1
GM1
Yptb WT
siCD59

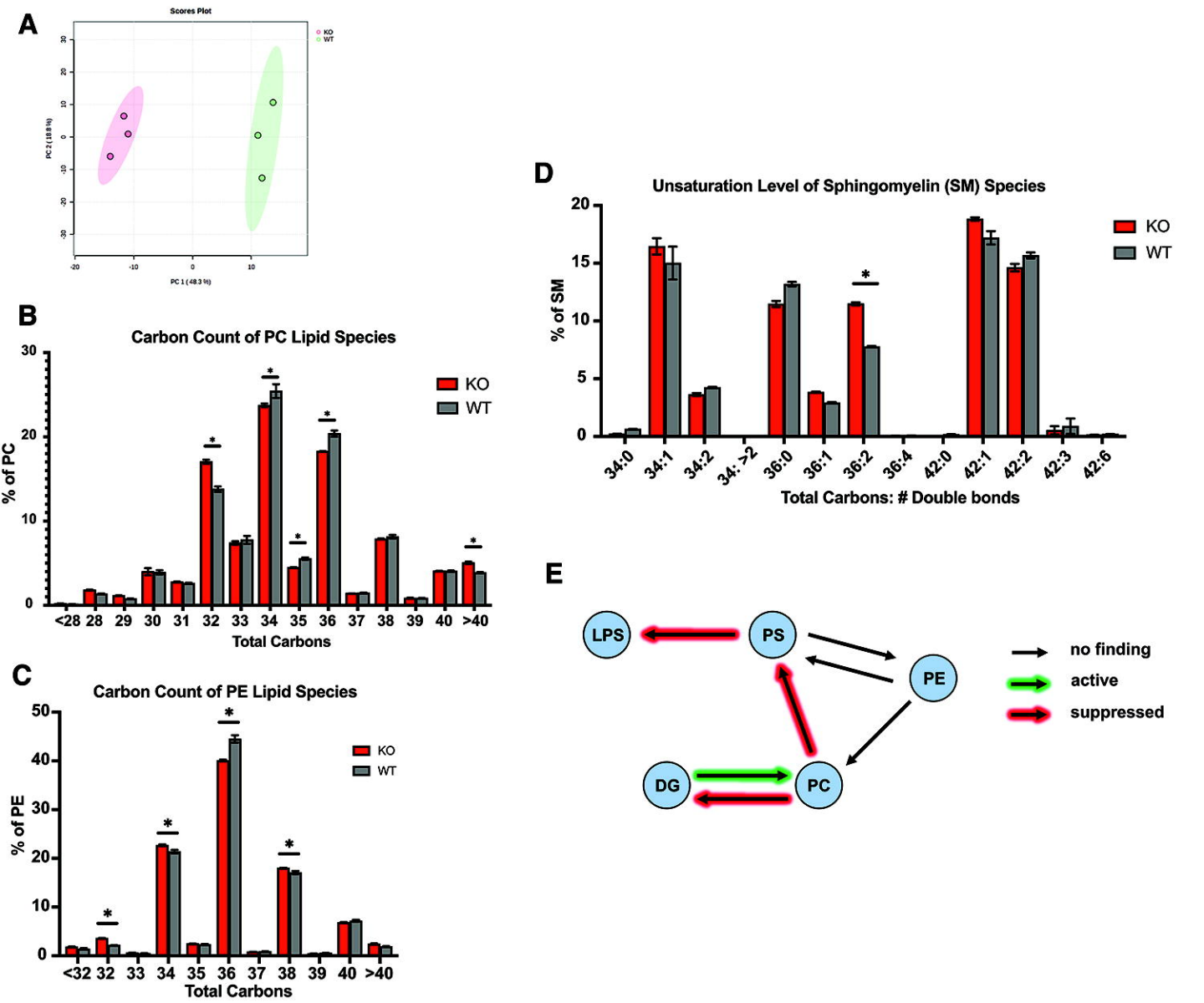
A
Scores Plot
KO
WT
PC 2 (18.8 %)
PC 1 (48.3 %)
B
Carbon Count of PC Lipid Species
% of PC
KO
WT
<28 28 29 30 31 32 33 34 35 36 37 38 39 40 >40
Total Carbons
C
Carbon Count of PE Lipid Species
% of PE
KO
WT
<32 32 33 34 35 36 37 38 39 40 >40
Total Carbons
D
Unsaturation Level of Sphingomyelin (SM) Species
% of SM
KO
WT
34:0 34:1 34:2 34: >2 36:0 36:1 36:2 36:4 42:0 42:1 42:2 42:3 42:6
Total Carbons: # Double bonds
E
LPS
PS
PE
DG
PC
no finding
active
suppressed